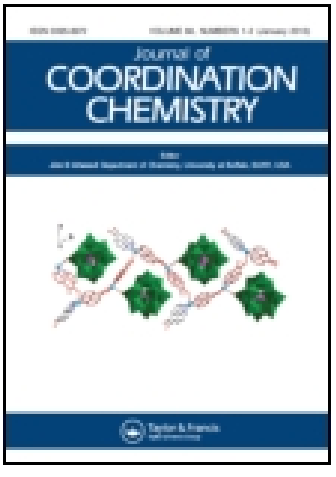




Journal of Coordination Chemistry
Publication details, including instructions for authors and subscription information:
http://www.tandfonline.com/loi/gcoo20

# A series of $Zn^{II}$ and $Co^{II}$ complexes based on 2-(imidazo[1,5-a]pyridin-3-yl)phenol: syntheses, structures, and luminescent and magnetic properties

Qian Gao[a], Yanmei Chen[ab], Yonglu Liu[a], Cong Li[a], Dandan Gao[b], Bing Wu[a], Haiyan Li[a], Yahong Li[ac], Wei Liu[a] & Wu Li[b]

[a] Key Laboratory of Organic Synthesis of Jiangsu Province, College of Chemistry, Chemical Engineering and Materials Science, Soochow University, Suzhou, China

[b] Key Laboratory of Salt Lake Resources and Chemistry, Qinghai Institute of Salt Lakes, Chinese Academy of Sciences, Xining, China

[c] State Key Laboratory of Applied Organic Chemistry, Lanzhou University, Lanzhou, China

Accepted author version posted online: 30 May 2014.Published online: 26 Jun 2014.

To cite this article: Qian Gao, Yanmei Chen, Yonglu Liu, Cong Li, Dandan Gao, Bing Wu, Haiyan Li, Yahong Li, Wei Liu & Wu Li (2014) A series of $Zn^{II}$ and $Co^{II}$ complexes based on 2-(imidazo[1,5-a]pyridin-3-yl)phenol: syntheses, structures, and luminescent and magnetic properties, Journal of Coordination Chemistry, 67:10, 1673-1692, DOI: 10.1080/00958972.2014.927061

To link to this article: http://dx.doi.org/10.1080/00958972.2014.927061

*Journal of Coordination Chemistry*, 2014
Vol. 67, No. 10, 1673–1692, http://dx.doi.org/10.1080/00958972.2014.927061





# A series of $Zn^{II}$ and $Co^{II}$ complexes based on 2-(imidazo[1,5-a]pyridin-3-yl)phenol: syntheses, structures, and luminescent and magnetic properties

QIAN GAO†, YANMEI CHEN†‡, YONGLU LIU†, CONG LI†, DANDAN GAO‡, BING WU†, HAIYAN LI†, YAHONG LI*†§, WEI LIU**† and WU LI‡

†Key Laboratory of Organic Synthesis of Jiangsu Province, College of Chemistry, Chemical Engineering and Materials Science, Soochow University, Suzhou, China
‡Key Laboratory of Salt Lake Resources and Chemistry, Qinghai Institute of Salt Lakes, Chinese Academy of Sciences, Xining, China
§State Key Laboratory of Applied Organic Chemistry, Lanzhou University, Lanzhou, China

(*Received 7 December 2013; accepted 1 April 2014*)

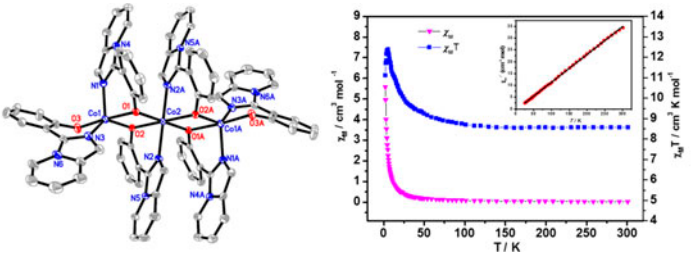


Five coordination complexes based on 2-(imidazo[1,5-a]pyridin-3-yl)phenol were synthesized and characterized; their luminescent and magnetic properties were studied.

The employment of 2-(imidazo[1,5-a]pyridin-3-yl)phenol (HIPP) in $Zn^{II}$ and $Co^{II}$ coordination chemistry is reported. A series of complexes of compositions, $[Zn(HIPP)_2Cl_2]$ (**1**), $[Zn_2(IPP)_4]$ (**2**), $[Co_2(HIPP)_4(SO_4)_2]$ (**3**), $[Co_3(IPP)_6]$ (**4**), and $[Co_2(IPP)_2(CH_3COO)_2]_n$ (**5**), have been synthesized via choosing appropriate metal salts and different solvents. Complexes of various nuclearities are obtained from mono-, di-, trinuclear complexes to 1-D chain polymer. UV–vis absorption properties have been investigated and rationalized by density functional theory and time-dependent DFT calculations. In addition, luminescence studies suggested strong emissions for **1**, **2**, and **3** in the solid state at room temperature. Variable temperature (2.0–300 K) magnetic studies for **3**, **4**, and **5** indicate weak antiferromagnetic coupling between the metal centers in **3** and **5**, and weak ferromagnetic $Co^{II}\cdots Co^{II}$ exchange interactions in **4**.

*Keywords*: Crystal structures; 2-(Imidazo[1, 5-a]pyridin-3-yl)phenol; DFT and TDDFT calculations; Luminescent properties; Magnetic properties

*Corresponding authors. Email: liyahong@suda.edu.cn (Y. Li); weiliu@suda.edu.cn (W. Liu)

## 1. Introduction

Attention has been given to the bicyclic heteroaromatic imidazo[1,5-a]pyridine family of molecules and ligands. Important research areas include potential applications in organic light-emitting diodes [1, 2] and organic thin-layer field effect transistors [3]. Moreover, imidazo[1,5-a]pyridine and its derivatives have been investigated as pharmaceuticals [4–7] and as precursors of N-heterocyclic carbenes [8–10]. Despite this interest, coordination complexes of imidazo[1,5-*a*]pyridine and its derivatives are exceedingly rare. Only a few examples of $Cu^{II}$ [11–13], $Co^{II}$ [14], $V^{V}$ [15], $Mn^{II}$ [16], and $Re^{I}$ [1] complexes have been reported. Hence, the development of efficient access to these complexes is in high demand.

In previous reports, a powerful strategy for the synthesis of iron, cobalt, and copper complexes supported by *in situ* generated derivatives of imidazo[1,5-a]pyridine ligands was described [12, 13]. As a continuation of our previous studies, we investigated 2-(imidazo [1,5-a]pyridin-3-yl)phenol (HIPP) in the formation of $Zn^{II}$ and $Co^{II}$ coordination complexes. HIPP, as a derivative of imidazo[1,5-a]pyridine, is heteroaromatic $\pi$-electron efficient and can be a good candidate for constructing interesting supramolecular networks. It potentially offers reactive sites at both N and OH groups, and binds to metal ions in various coordination modes. Although the synthesis of HIPP has been reported [17], it has never been utilized as a ligand to prepare coordination complexes.

In the present study, five complexes, $[Zn(HIPP)_2Cl_2]$ (**1**), $[Zn_2(IPP)_4]$ (**2**), $[Co_2(HIPP)_4(SO_4)_2]$ (**3**), $[Co_3(IPP)_6]$ (**4**), and $[Co_2(IPP)_2(CH_3COO)_2]_n$ (**5**), have been synthesized under solvothermal conditions. The absorption properties are discussed on the basis of density functional theory (DFT) and time-dependent DFT (TDDFT) calculations. The luminescent and magnetic properties of these complexes are also studied.

## 2. Experimental

### 2.1. *General considerations*

All manipulations were performed under aerobic and solvothermal conditions using reagents and solvents, as received. The C, H, and N microanalyses were carried out with a Carlo-Erba EA1110 CHNO-S elemental analyzer. FT-IR spectra were recorded as KBr pellets from 400 to 4000 $cm^{-1}$ on a Nicolet MagNa-IR 500 spectrometer. Powder X-ray diffraction (PXRD) was recorded on a Rigaku D/Max-2500 diffractometer at 40 kV and 100 Ma with a Cu-target tube and a graphite monochromator. Absorption spectra were recorded with a JASCO V-570 spectrophotometer at room temperature. Emission spectra were measured on an FLsp920 fluorescence spectrometer. Variable-temperature dc magnetic susceptibility data were collected using a Quantum Design MPMS-7 SQUID magnetometer. The synthesis of HIPP is different from that described in the literature [17]. We prepared the ligand by using salicylic acid, 2-methylaminopyridine, and propane phosphoric acid anhydride ($T_3P$).

### 2.2. *Syntheses*

**2.2.1. Synthesis of HIPP.** To a solution of salicylic acid (2.76 g, 20 mM) in n-butyl acetate (40 mL) at room temperature, 2-methylaminopyridine (2.16 g, 20 mM) and $T_3P$ were

added, resulting in the formation of a yellow mixture. After being stirred at 120 °C for 3 h, the mixture was then cooled to room temperature, neutralized by ammonia solution, and extracted with ethyl acetate (2 × 40 mL). The combined organic layers were dried over anhydrous magnesium sulfate, filtered, and concentrated *in vacuo*. The crude product was purified by column chromatography on silica gel with an eluent of 1 : 4 ethyl acetate/petroleum ether (v/v) to give pure HIPP as a yellow solid. Yield: 75%. Anal. Calcd for $C_{13}H_{10}N_2O$ (%): C, 74.27; H, 4.79; N, 13.33. Found (%): C, 74.11; H, 4.68; N, 13.20. Selected IR data (KBr, $cm^{-1}$): 2554 (w), 1514 (s), 1450 (s), 1383 (s), 1296 (s), 1234 (m), 1091 (s), 1000 (s), 932 (s), 734 (s). $^1H$ NMR (400 MHz, $CDCl_3$), $\delta$ 11.82 (1H, s), 8.52 (1H, d, $J = 6.8$), 7.77 (1H, d, $J = 7.7$), 7.54 (2H, d, $J = 14.0$), 7.30 (1H, d, $J = 7.3$), 7.17 (1H, d, $J = 8.0$), 7.01 (1H, t, $J = 7.4$), 6.80 (1H, d, $J = 6.9$), 6.68 (1H, s).

**2.2.2. Synthesis of $[Zn(HIPP)_2Cl_2]$ (1).** A mixture of HIPP (20.7 mg, 0.1 mM), $ZnCl_2 \cdot 2H_2O$ (13.6 mg, 0.1 mM), and $CH_3CH_2OH$ (1 mL) was sealed in a Pyrex-tube (8 mL). The tube was heated at 80 °C for four days under autogenous pressure. Cooling of the resultant solution to room temperature gave pale-yellow crystals. The crystals were collected by filtration, washed with $CH_3CH_2OH$ (2 mL), and dried in air. Yield: 0.0278 g (50%, based on Zn). Anal. Calcd for $C_{26}H_{20}Cl_2N_4O_2Zn$ (%): C, 56.09; H, 3.62; N, 10.06. Found (%): C, 55.87; H, 3.64; N, 9.96. Selected IR data (KBr, $cm^{-1}$): 3376 (s), 1610 (s), 1519 (s), 1472 (s), 1451 (s), 1213 (s), 1289 (m), 1005 (s), 917 (s), 829 (s), 763 (s), 687 (s).

**2.2.3. Synthesis of $[Zn_2(IPP)_4]$ (2).** A mixture of HIPP (20.7 mg, 0.1 mM), Zn $(CH_3COO)_2 \cdot 2H_2O$ (10.8 mg, 0.05 mM), and $CH_3CH_2OH$ (1 mL) was sealed in a Pyrex-tube (8 mL). The tube was heated at 120 °C for three days under autogenous pressure. Cooling of the resultant solution to room temperature gave yellow block crystals. The crystals were collected by filtration, washed with $CH_3CH_2OH$ (2 mL), and dried in air. Yield: 0.0145 g (60%, based on Zn). Anal. Calcd for $C_{52}H_{36}N_8O_4Zn_2$ (%): C, 64.54; H, 3.75; N, 11.58. Found (%): C, 64.08; H, 3.64; N, 11.32. Selected IR data (KBr, $cm^{-1}$): 1596 (s), 1471 (s), 1442 (m), 1295 (s), 1268 (m), 1122 (m), 1002 (w), 841 (s), 751 (w), 689 (s).

**2.2.4. Synthesis of $[Co_2(HIPP)_4(SO_4)_2]$ (3).** A mixture of HIPP (20.7 mg, 0.1 mM), $CoSO_4 \cdot 7H_2O$ (14.0 mg, 0.05 mM), and $CH_3CH_2OH$ (1 mL) was sealed in a Pyrex-tube (8 mL). The tube was heated at 80 °C for 4 days under autogenous pressure. Cooling of the resultant solution to room temperature gave purple block crystals. The crystals were collected by filtration, washed with $CH_3CH_2OH$ (3 mL) and dried in air. Yield: 0.0115 g (40%, based on Co). Anal. Calcd for $C_{52}H_{40}Co_2N_8O_{12}S_2$ (%): C, 54.27; H, 3.50; N, 9.74. Found (%): C, 53.77; H, 3.64; N, 9.52. Selected IR data (KBr, $cm^{-1}$): 3231 (m), 1589 (m), 1517 (m), 1452 (s), 1299 (m), 1219 (s), 1066 (s), 998 (m), 833 (m), 763 (s), 688 (m).

**2.2.5. Synthesis of $[Co_3(IPP)_6]$ (4).** A mixture of HIPP (20.7 mg, 0.1 mM), Co $(CH_3COO)_2 \cdot 4H_2O$ (12.5 mg, 0.05 mM), and DMF (1 mL) was sealed in a Pyrex-tube (8 mL). The tube was heated at 100 °C for 14 days under autogenous pressure. Cooling of the resultant solution to room temperature gave orange block crystals. The crystals were collected by filtration, washed with DMF (2 mL), and dried in air. Yield: 0.0086 g (36%, based on Co). Anal. Calcd for $C_{78}H_{54}Co_3N_{12}O_6$ (%): C, 65.42; H, 3.80; N, 11.74. Found (%): C,

65.25; H, 3.79; N, 11.68. Selected IR data (KBr, $cm^{-1}$): 1597 (s), 1470 (s), 1443 (s), 1303 (s), 1267 (s), 1122 (s), 1004 (m), 908 (m), 842 (s), 734 (s), 725 (s), 714 (s), 685 (s).

**2.2.6. Synthesis of $[Co_2(IPP)_2(CH_3COO)_2]_n$ (5).** A mixture of HIPP (20.7 mg, 0.1 mM), $Co(CH_3COO)_2{\cdot}4H_2O$ (24.9 mg, 0.1 mM), and $CH_3CH_2OH$ (1 mL) was sealed in a Pyrex-tube (8 mL). The tube was heated at 90 °C for six days under autogenous pressure. Cooling of the resultant solution to room temperature gave purple block crystals. The crystals were collected by filtration, washed with $CH_3CH_2OH$ (2 mL), and dried in air. Yield: 0.0098 g (30%, based on Co). Anal. Calcd for $C_{30}H_{24}Co_2N_4O_6$ (%): C, 55.06; H, 3.70; N, 8.56. Found (%): C, 54.38; H, 3.62; N, 8.34. Selected IR data (KBr, $cm^{-1}$): 1606 (s), 1572 (s), 1472 (s), 1294 (m), 1247 (m), 1124 (m), 1005 (w), 844 (m), 763 (m), 689 (m).

### 2.3. *X-ray diffraction crystallography*

Data were collected at room temperature on a Bruker Smart ApexII diffractometer for **1**, **3**, **4**, and **5** and on a Rigaku Mercury CCD X-ray diffractometer for **2** utilizing Mo K$\alpha$ radiation ($\lambda = 0.71073$ Å); the $\omega$-and-$\varphi$ scan technique was applied. The structures were solved by direct methods using SHELXS-97 [18]. Non-hydrogen atoms were refined anisotropically by full-matrix least-squares calculations on $F^2$ [19]. Hydrogens were placed geometrically and constrained using a riding model. Crystallographic data together with refinement details for the new complexes reported in this work are summarized in table 1. Selected bond lengths and angles for **1**–**5** are given in Supplementary material.

### 2.4. *Computational details*

All calculations were carried out with Gaussian03 programs [20]. DFT and TDDFT with the three-parameter hybrid functional (B3LYP) were employed [21–23]. A combined basis set of 6-31G* with the LANL2DZ effective core potentials (ECP) has been widely used for transition metal complexes [24–26]. Our calculations were carried out using a 6-31G* basis set for C, H, N, O, and Cl atoms and LANL2DZ for Zn [27–30]. All geometries were characterized as minima by frequency analysis ($N_{imag} = 0$).

## 3. Results and discussion

### 3.1. *Synthesis and IR spectra*

The ligand HIPP was prepared by a one-pot synthesis [31], which was accessed by using salicylic acid, 2-methylaminopyridine, and propane phosphoric acid anhydride ($T_3P$). Compared with the previously reported synthesis, this method is more efficient and convenient and can afford a higher yield.

Pale-yellow crystals of **1** were prepared by heating a mixture of HIPP and $ZnCl_2{\cdot}2H_2O$ under solvothermal conditions in ethanol at 80 °C for four days.

Motivated by the successful preparation of the mononuclear $Zn^{II}$ complex supported by HIPP via solvothermal reaction, we next attempted to utilize $Zn(CH_3COO)_2{\cdot}2H_2O$ instead of $ZnCl_2{\cdot}2H_2O$ to synthesize other $Zn^{II}$ complexes. To our delight, the reaction of HIPP and $Zn(CH_3COO)_2{\cdot}2H_2O$ in ethanol at 120 °C afforded dinuclear $[Zn_2(IPP)_4]$ (**2**).

Table 1. Crystal data and structure refinement for **1–5**.

| | **1** | **2** | **3** | **4** | **5** |
|---|---|---|---|---|---|
| Formula[a] | $C_{26}H_{20}Cl_2N_4O_2Zn$ | $C_{52}H_{36}N_8O_4Zn_2$ | $C_{52}H_{40}Co_2N_8O_{12}S_2$ | $C_{78}H_{54}Co_3N_{12}O_6$ | $C_{30}H_{24}Co_2N_4O_6$ |
| $M$ ($gM^{-1}$)[a] | 556.75 | 967.67 | 1150.9 | 1432.12 | 654.39 |
| $T$ (K) | 296(2) | 223(2) | 296(2) | 296(2) | 296(2) |
| $\lambda$ (Å)[b] | 0.71073 | 0.71073 | 0.71073 | 0.71073 | 0.71073 |
| Crystal system | Monoclinic | Triclinic | Monoclinic | Triclinic | Monoclinic |
| Space group | *C2/c* | *P*$\bar{1}$ | $P2_1/n$ | *P*$\bar{1}$ | $P2_1/c$ |
| $a$ (Å) | 7.1656(8) | 9.856(2) | 11.4242(9) | 11.638(3) | 13.392(6) |
| $b$ (Å) | 18.090(2) | 11.727(2) | 15.7200(13) | 11.8862(15) | 19.149(9) |
| $c$ (Å) | 18.9412(18) | 18.800(4) | 13.6497(11) | 13.4287(17) | 11.433(5) |
| $\alpha$ (°) | 90.00 | 80.83(3) | 90.00 | 112.899(2) | 90.00 |
| $\beta$ (°) | 92.477(2) | 84.42(3) | 91.2450(10) | 110.410(3) | 98.441(8) |
| $\gamma$ (°) | 90.00 | 79.52(3) | 90.00 | 94.947(3) | 90.00 |
| $V$ ($Å^3$) | 2453.0(5) | 2104.2(7) | 2450.7(3) | 1549.9(5) | 2900(2) |
| $Z$ | 4 | 2 | 2 | 1 | 4 |
| $\rho_c$ ($g\,cm^{-3}$) | 1.508 | 1.527 | 1.560 | 1.534 | 1.499 |
| $\mu$ ($mm^{-1}$) | 1.251 | 1.200 | 0.837 | 0.864 | 1.193 |
| $F$ (0 0 0) | 1136 | 992 | 1180 | 735 | 1336 |
| $\theta$ Range (°) | 2.15–28.69 | 3.03–27.48 | 1.98–28.31 | 1.81–25.00 | 2.09–28.52 |
| Measd/independent | 8710/3131 | 19,411/9472 | 16,762/6067 | 8423/5321 | 20,169/7234 |
| $R_{int}$ reflections | 0.0240 | 0.0421 | 0.0190 | 0.0226 | 0.0555 |
| Obsd reflns [$I > 2\sigma(I)$] | 3131 | 9472 | 6067 | 5321 | 7234 |
| GOF on $F^2$ | 1.126 | 1.068 | 1.022 | 1.062 | 1.030 |
| $R_1$[c] | 0.0292 | 0.0619 | 0.0291 | 0.0381 | 0.0605 |
| $wR_2$[d,e] | 0.0806 | 0.1149 | 0.0761 | 0.1168 | 0.1460 |
| $(\Delta\rho)_{max,min}$ (e $Å^{-3}$) | 0.509, −0.342 | 0.442, −0.450 | 0.300, −0.294 | 0.337, −0.355 | 1.044, −0.880 |

[a]Including solvate molecules.
[b]Mo K$\alpha$ radiation.
[c]$R_1 = \Sigma(|F_o| - |F_c|)/\Sigma(|F_o|)$ for observed reflections.
[d]$w = 1/[\sigma^2(F_o^2) + (\alpha P)^2 + bP]$ and $P = [\max(F_o^2,0) + 2F_c^2]/3$.
[e]$wR_2 = \{\Sigma[w(F_o^2 - F_c^2)^2]/\Sigma[w(F_o^2)^2]\}^{1/2}$ for all data.

The treatment of $CoSO_4 \cdot 7H_2O$ with HIPP in ethanol gave a dinuclear complex $[Co_2(HIPP)_4(SO_4)_2]$ (**3**). The reaction of $Co(CH_3COO)_2 \cdot 4H_2O$ and HIPP in DMF produced a trinuclear complex $[Co_3(IPP)_6]$ (**4**). When the reaction of $Co(CH_3COO)_2 \cdot 4H_2O$ and HIPP was conducted in ethanol, a coordination polymer $[Co_2(IPP)_2(CH_3COO)_2]_n$ (**5**) was obtained. The syntheses of **1–5** are listed in scheme 1.

The generation of **1–5** indicates that the structures of $Zn^{II}$ and $Co^{II}$ complexes based on HIPP could be assembled via choosing different metal salts and employing the appropriate solvents, reflecting the synthetic novelty and importance of this work.

For **1** and **3**, the presence of HIPP is manifested by a broad IR band of medium intensity at 3200–3400 $cm^{-1}$, which can be assigned to $\nu$(OH). A sharp band at 1600 $cm^{-1}$ can be ascribed to the $\nu_{as}$(C=N) vibration. Several bands at 1480–1011 $cm^{-1}$ could be assigned as stretching vibrations of the pyridine ring. IR spectra of **2**, **4**, and **5** contain all of the pertinent bands of $IPP^-$, e.g. 1600, 1470, 1442, 1330, 1250 $cm^{-1}$, etc.

### 3.2. *Structural descriptions of 1–5*

**3.2.1. Structure description of $[Zn(HIPP)_2Cl_2]$ (1).** Complex **1** crystallizes in the monoclinic crystal system of the *C2/c* space group. It consists of one $Zn^{II}$, two HIPP ligands, and

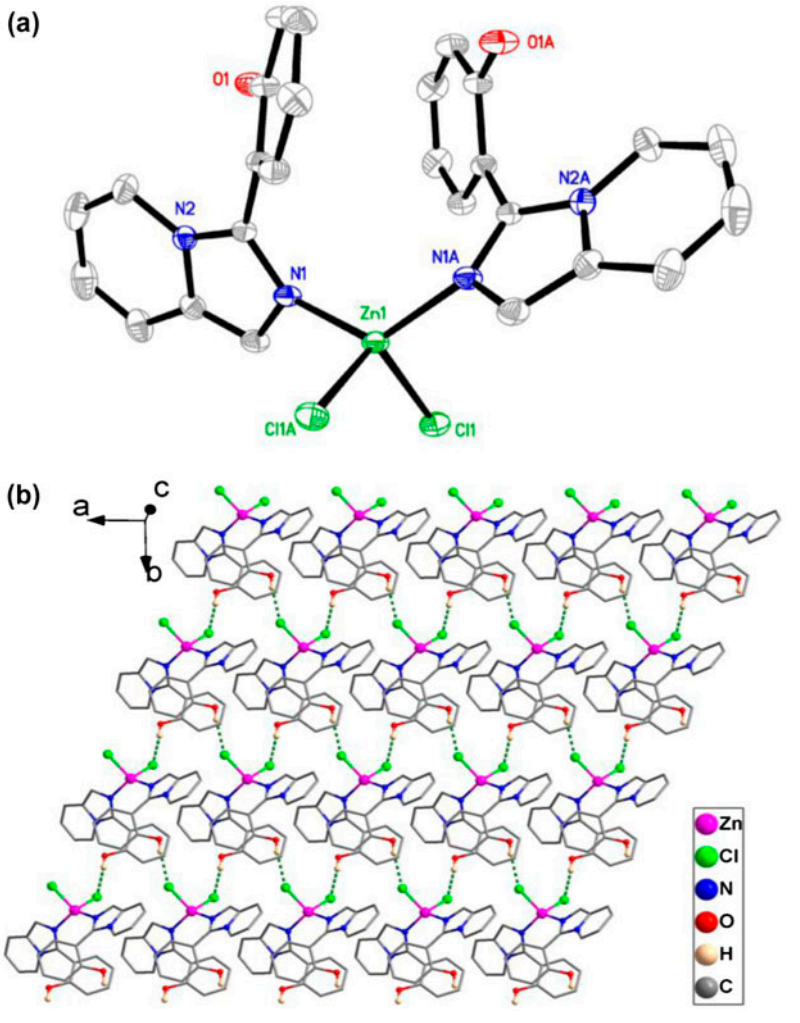


Figure 1. (a) Labeled ORTEP plot at the 30% ellipsoid level of $[Zn(HIPP)_2Cl_2]$ (**1**). Hydrogens have been omitted for clarity. (b) The 2-D structure created by intermolecular hydrogen bonds (some hydrogen bonds are omitted for clarity).

two chlorides [figure 1(a)]. Zn1 is surrounded by two nitrogens and two chlorides in a distorted tetrahedral geometry. The bond distances of Zn–N and Zn–Cl are 2.004(2) and 2.282 (5) Å, respectively. Both the Zn–N and Zn–Cl bonds are in good agreement with the reported values (2.023 ± 0.033 Å for Zn–N and 2.253 ± 0.033 Å for Zn–Cl) [32]. The HIPP ligands coordinate to $Zn^{II}$ through nitrogen from the imidazole in $\eta^1$ coordination (scheme 2). Based on the relative orientation of the phenol oxygen and the coordinated imidazole nitrogen, the ligands adopt the *anti* conformation, while the phenol rings in HIPP ligands are largely twisted from the imidazo[1,5-a]pyridine rings, with the dihedral angle of 53.39 (5)°. The intermolecular hydrogen bonds between OH of the ligands as hydrogen donors and chloride as acceptors were determined in this complex (table 2). These intermolecular hydrogen contacts connect the molecules to generate a 2-D network structure [figure 1(b)].

Table 2. Intermolecular hydrogen bond lengths and angles for **1**, **3** and **5**.

| D–H···A | d(D–H) | d(H···A) | D(D···A) | < (DHA) |
|---|---|---|---|---|
| **1** | | | | |
| O(1)–H(1A)···Cl(1)B | 0.82 | 2.38 | 3.188(1) | 168.7 |
| **3** | | | | |
| O(5)–H(5)···O(4)B | 0.82 | 1.90 | 2.699(2) | 164.9 |
| O(6)–H(6)···O(4)B | 0.82 | 1.94 | 2.752(2) | 169.0 |
| C(12)–H(12)···O(1)B | 0.93 | 2.49 | 3.373(2) | 157.9 |
| **5** | | | | |
| C(18)–H(18)···O(3)C | 0.93 | 2.57 | 3.466(7) | 161.1 |

Note: Symmetry transformations used to generate equivalent atoms: B: $-x+1/2, y+1/2, -z+1/2$ for **1**; B: $x+1/2, -y+1/2, z+1/2$ for **2**; C: $x, y, -1+z$ for **3**.

**3.2.2. Structure description of $[Zn_2(IPP)_4]$ (2).** The perspective view of the molecular structure of **2** with an atomic labeling scheme is shown in figure 2. The compound crystallizes in the triclinic crystal system of space group $P\bar{1}$. The asymmetric unit consists of two $Zn^{II}$ ions and four $IPP^-$ ligands. Zn1 is five-coordinate, from two nitrogens and three oxygens from three $IPP^-$ ligands to form a distorted tetragonal pyramidal geometry [figure 2(a)], with the structural parameter of $\tau = 0.26$, and $\tau = |\beta - \alpha|/60$, where $\alpha$ and $\beta$ are

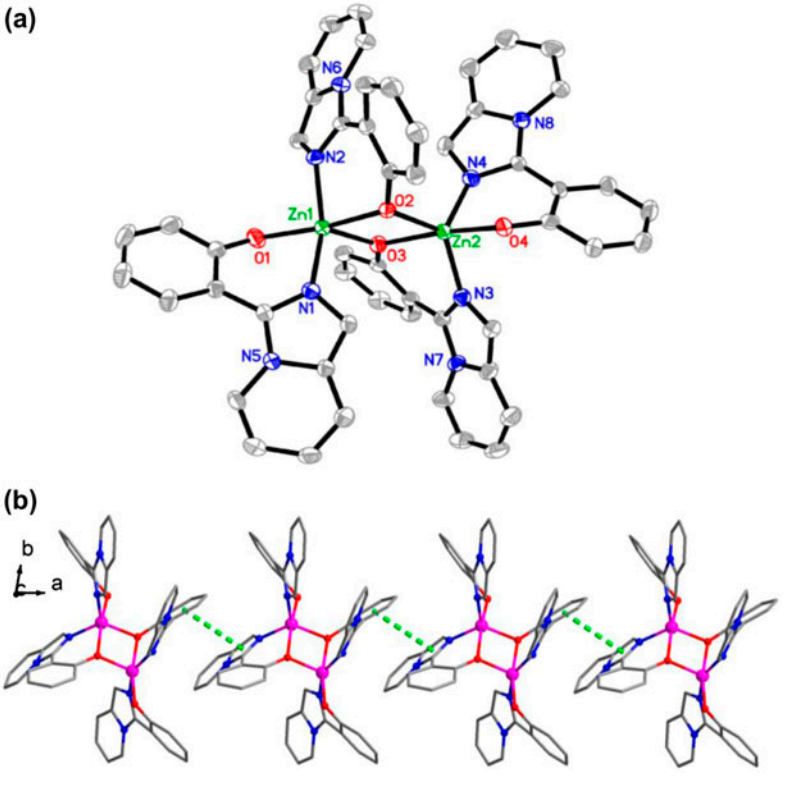


Figure 2. (a) Labeled ORTEP plot at the 30% ellipsoid level of $[Zn_2(IPP)_4]$ (**2**). Hydrogens have been omitted for clarity. (b) Crystal packing diagram of **2**. The $\pi\cdots\pi$ stacking interactions are represented by the dotted lines.

the largest angles around five-coordinate metal center, as reported by Addison *et al.* [33]. Zn2 is encircled by two nitrogens from two $IPP^-$ ligands and three phenol oxygens, resulting in five-coordinate $[ZnN_2O_3]$ with distorted trigonal bipyramidal geometry ($\tau = 0.68$). The Zn–N bonds in this complex are 2.023(3)–2.053(3) Å, which are slightly shorter than the previously reported Zn(II) complex [34]. Unlike the coordination mode in **1**, the deprotonated $IPP^-$ ligands adopt a $\mu_2$-bridging mode to link two $Zn^{II}$ ions in a $\mu_2:\eta^1:\eta^2$ mode (scheme 2), and the two ligands in **2** adopt the *syn* conformation. Consequently, the phenolate rings in $IPP^-$ are slightly twisted from the imidazo[1,5-a]pyridine rings, with an average dihedral angle of 36.65(5)°. Strong intermolecular $\pi\cdots\pi$ stacking interactions with a centroid-to-centroid distance of 3.798 Å between the imidazole and pyridine rings occur, generating a 1-D chain structure [figure 2(b)].

**3.2.3. Structure description of $[Co_2(HIPP)_4(SO_4)_2]$ (3).** Complex **3** crystallizes in the monoclinic crystal system of the $P\bar{1}$ space group. X-ray single crystal analysis indicates that the complex consists of two $Co^{2+}$ ions, four HIPP ligands, and two $SO_4^{2-}$ anions. Each cobalt ion is coordinated by two nitrogens from two HIPP ligands and two oxygens from two sulfates to form a distorted tetrahedral geometry [figure 3(a)]. Each HIPP coordinates to $Co^{II}$ through the nitrogen of the imidazole in $\eta^1$ coordination (scheme 1). Two sulfates bridge two $[Co(HIPP)_2]^{2+}$ moieties in the coordination mode of $\mu_2:\eta^1:\eta^1$ to form a dinuclear structure. The uncoordinated S–O bond lengths (S1–O3 = 1.437(13) Å, S1–O4 = 1.461 (12) Å) are slightly shorter than those of the coordinated S–O bond lengths (S1–O1 = 1.486 (13) Å, S1–O2 = 1.481(12) Å). As shown in figure 3(b) and table 2, complex **3** features intermolecular O–H···O hydrogen contacts between OH of phenol rings as hydrogen donors and oxygen from $SO_4^{2-}$ anions as acceptors (O5–H5···O4B, O to O distance 2.699(2) Å, O5–H5···O4B angle 164.9°; O6–H6···O4B, O to O distance 2.752(2) Å, O6–H6···O4B angle 169.0°). In addition, weak intermolecular C–H···O contacts (C(12)–H(12)···O(1)B, C to O distance 3.373(2) Å, C(12)–H(12)···O(1)B angle 157.9°) are observed from the CH groups of the phenol rings (donors) to the coordinated oxygens (acceptors) from sulfates (table 2). These intermolecular hydrogen contacts connect the molecules to generate an infinite 2-D network.

**3.2.4. Structure description of $[Co_3(IPP)_6]$ (4).** Single crystal X-ray diffraction reveals that **4** crystallizes in the triclinic system of the space group $P\bar{1}$. The asymmetric unit consists of two crystallographically independent $Co^{II}$ ions and three $IPP^-$ ligands. Co1A is generated by a symmetry operation. The terminal Co1 is coordinated by two nitrogens from two $IPP^-$ ligands and three phenyl oxygens, resulting in the five-coordinate $[CoN_2O_3]$ environment with distorted square pyramidal geometry ($\tau = 0.70$). Co2 ion is coordinated by four oxygens (O1, O2, O1A, and O2A) from four $IPP^-$ ligands in the equatorial plane and two nitrogens (N2 and its equivalent N2A) in the axial positions to form a $[CoN_2O_4]$ octahedral geometry (figure 4). In this complex, $IPP^-$ coordinates to the metal ions in two modes, the terminal $IPP^-$ coordinates to $Co^{II}$ in the $\eta^1:\eta^1$, while the remaining four $IPP^-$ ligands are bidentate bridging spacers linking the adjacent $Co^{II}$ ions to generate two planar four-membered $[Co_2O_2]$ rings in the coordination mode of $\eta^1:\eta^1:\mu^2$ (scheme 1), and the adjacent $Co^{II}\cdots Co^{II}$ distance is 3.230(8) Å.

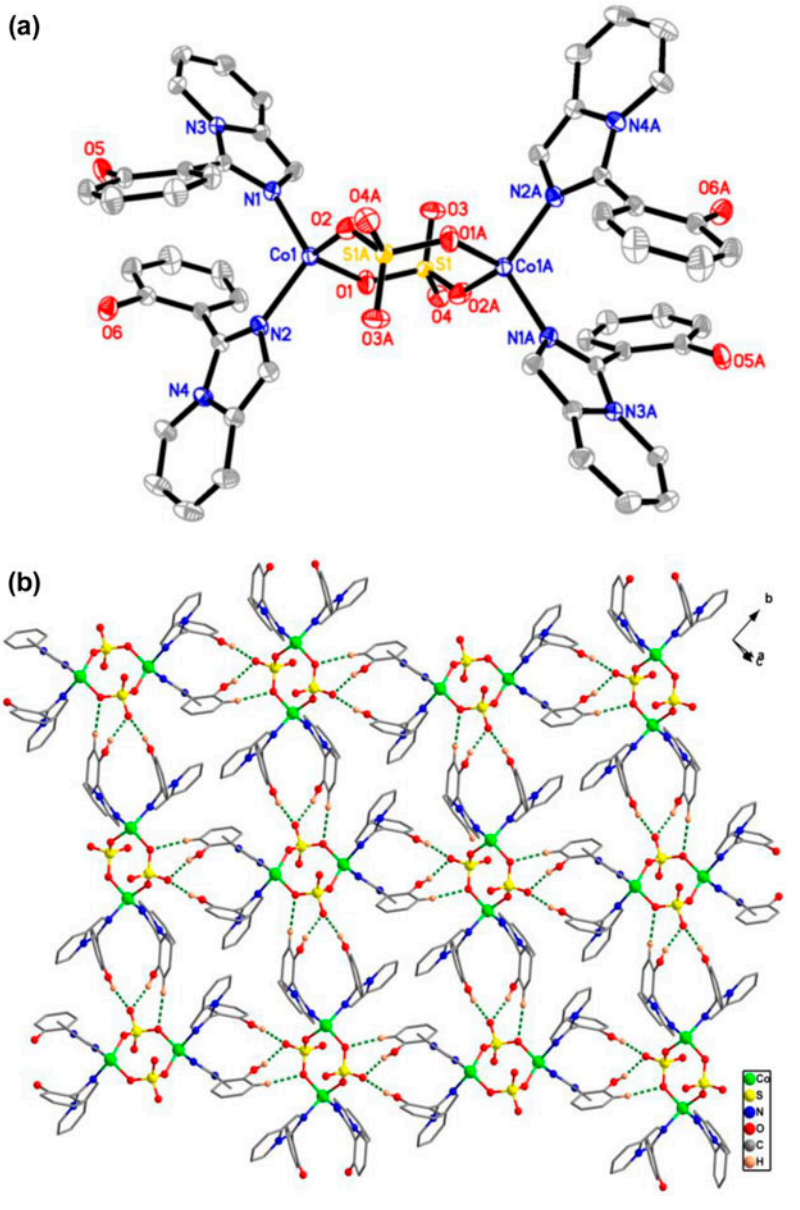


Figure 3. (a) Labeled ORTEP plot at the 30% ellipsoid level of $[Co_2(HIPP)_4(SO_4)_2]$ (**3**). Hydrogens have been omitted for clarity. (b) The 2-D structure created by intermolecular hydrogen bonds (some hydrogen bonds are omitted for clarity).

**3.2.5. Structure description of $[Co_2(IPP)_2(CH_3COO)_2]_n$ (5).** Crystal structure of **5** exhibits a chain structure. The asymmetric unit of **5** contains three crystallographically independent $Co^{II}$ ions (Co2 fully occupied, Co1, and Co3 half occupied), two $IPP^-$ anions, and two $CH_3COO^-$ anions [figure 5(a)]. The coordination environment around Co1 is best

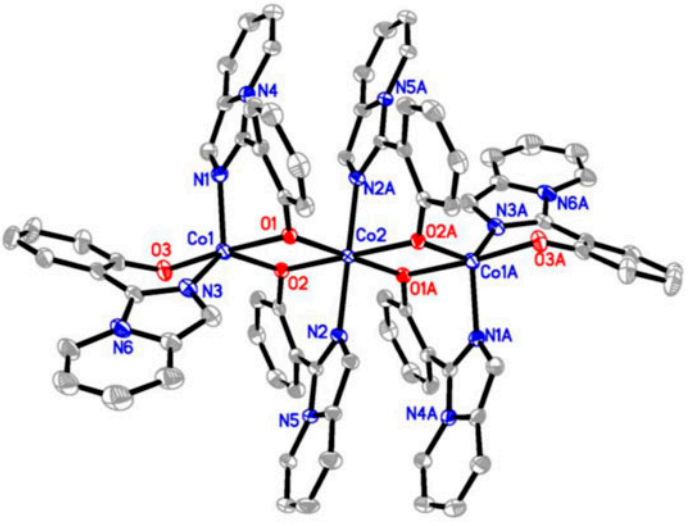


Figure 4. Labeled ORTEP plot at the 30% ellipsoid level of $[Co_3(IPP)_6]$ (**4**). Hydrogens have been omitted for clarity.

described as octahedral, in which the basal plane is occupied by four oxygens (O1, O2, O1A, and O2A) and the apical positions are occupied by two nitrogens from two $IPP^-$ anions. Co2 is bound to four oxygens and the coordination geometry of Co2 is best described as a distorted tetrahedron. The Co2–O distances range from 1.945(3) to 1.957(3) Å and the bond angles are from 105.32(1)° to 117.96(1)°. The coordination environment of Co3 is similar to that of Co1. The Co1, Co2, and Co3 sites are doubly bridged by phenol oxygens and the carboxylate oxygens to form a 1-D zigzag chain. Complex **5** features weak intermolecular C–H···O hydrogen contacts (C18–H18···O3C, C to O distance 3.466(7) Å, C18–H18···O3C angle 161.1°) between the CH groups of pyridine rings as hydrogen donors and oxygens from $CH_3COO^-$ of neighboring molecules as acceptors (table 2). These weak intermolecular hydrogen-bonding interactions connect the 1-D chains to afford a 2-D structure [figure 5(b)].

### 3.3. *Absorption and computational studies*

Absorption spectra of HIPP and **1**–**5** are shown in figure 6. For HIPP, the electronic spectrum displays intense absorption at 265–400 nm which are mainly comprised of several spin-allowed $n\rightarrow\pi^*$ and $\pi\rightarrow\pi^*$ transitions. The absorption bands of **1** and **3** are quite similar to that of the ligand, centered at 328 nm. For **2**, **4**, and **5**, a 10 nm red-shift of the absorption ($\lambda_{max} = 338$ nm) was observed. The red-shift may result from the deprotonation of phenol to phenolate groups of $IPP^-$ during coordination. Thus, such absorption can be tentatively attributed to $\pi\rightarrow\pi^*$ and $n\rightarrow\pi^*$ transitions.

In order to get a better understanding of the spectroscopic properties, complexes **1** and **2** are selected for DFT and TDDFT calculations in the gas phase. The metal–ligand bond lengths and angles in the optimized structures are quite similar to those obtained from single crystal determinations (tables 3 and 4), indicating that the structures are reproduced very

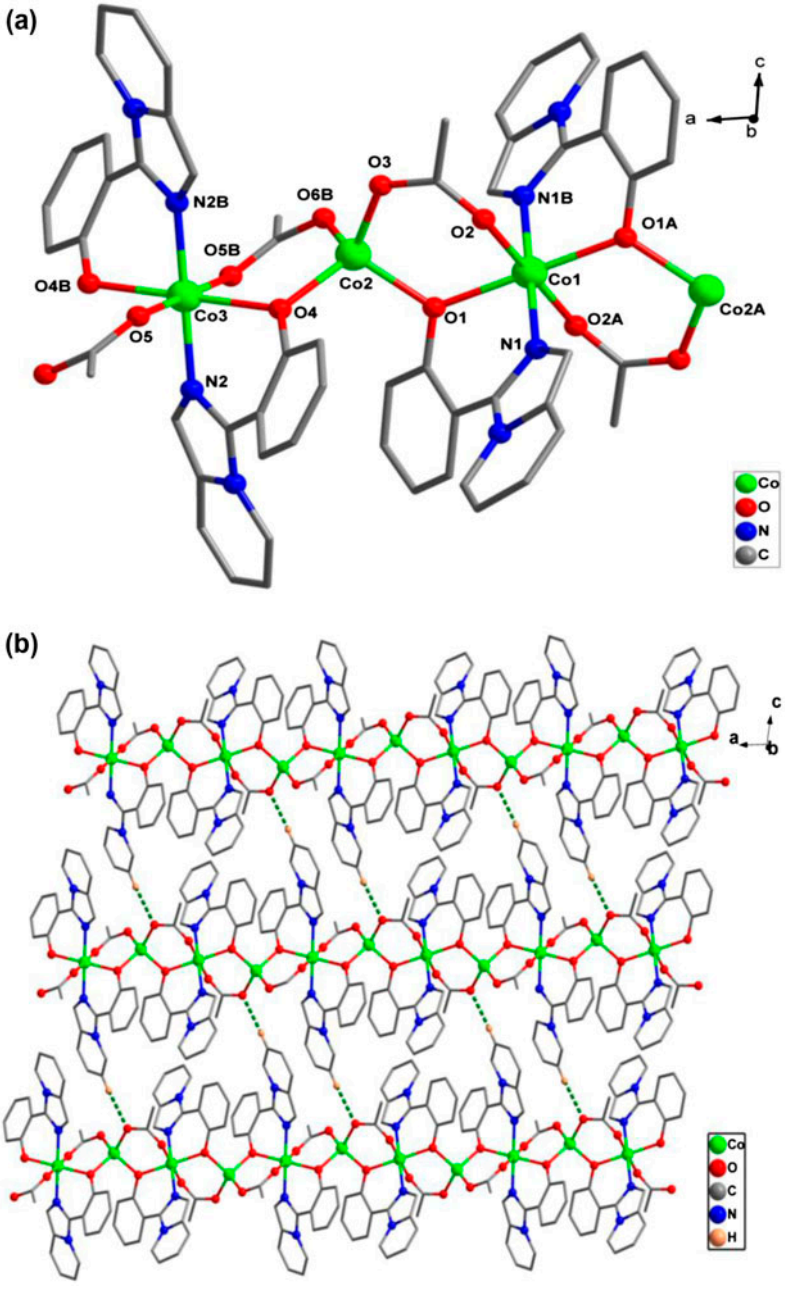


Figure 5. (a) Coordination environments of the $Co^{II}$ centers in $[Co_2(IPP)_2(CH_3COO)_2]_n$ (**5**). Hydrogens have been omitted for clarity. (b) The 2-D structure created by weak intermolecular hydrogen bonds (some hydrogen bonds are omitted for clarity).

well. The main optical transitions and molecular orbitals involved are presented in table 5, figures 7 and 8, while the calculated absorption spectra are shown in figure S1, see online supplemental material at http://dx.doi.org/10.1080/00958972.2014.927061.

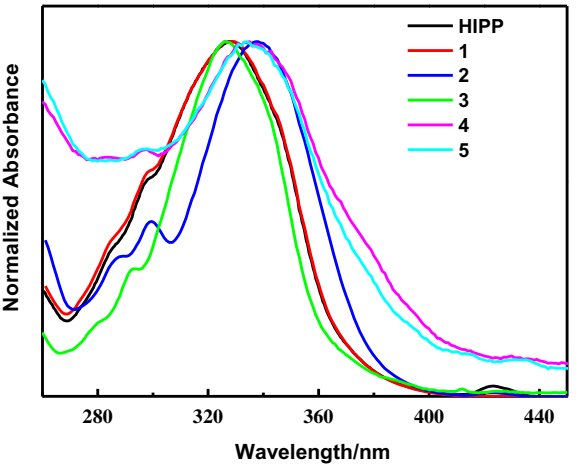


Figure 6. Normalized absorption spectra of HIPP and **1**–**5** in $CH_2Cl_2$ at room temperature.

Table 3. Selected experimental and calculated bond lengths (Å) and angles (°) for **1**.

| Bond length or angle | Exptl. | Calcd |
|---|---|---|
| Zn–Cl | 2.282(5) | 2.282 |
| Zn–$N_{HIPP}$ | 2.004(2) | 2.005 |
| Cl–Zn–Cl | 111.58(3) | 111.59 |
| $N_{HIPP}$–Zn–$N_{HIPP}$ | 125.80(8) | 125.78 |
| $\|\alpha\|$[a] | 53.39(5)° | 50.01 |

[a]Torsion angle between imidazo[1,5-a]pyridine and phenol rings in the HIPP ligand.

Table 4. Selected experimental and calculated bond lengths (Å) and angles (°) for **2**.

| Bond length or angle | Exptl. | Exptl. (average) | Calcd | Calcd (average) |
|---|---|---|---|---|
| Zn–$O_{terminal}$ | 2.012(3), 2.006(3) | 2.009(3) | 2.013, 2.013 | 2.013 |
| Zn–$O_{bridging}$ | 2.144(3), 2.125(3), 2.011(3), 1.972(3) | 2.063(3) | 2.139, 2.139, 2.060, 2.061 | 2.100 |
| Zn–$N_{IPP}^-$ | 2.053(3), 2.050(3), 2.047(4), 2.023(4) | 2.043(4) | 2.119, 2.119, 2.135, 2.135 | 2.127 |
| $N_{IPP}^-$–Zn–$O_{terminal}$ | 90.88(1), 93.66(1) | 92.27(1) | 89.43, 89.44 | 89.44 |
| $N_{IPP}^-$–Zn– $O_{bridging}$ | 83.35(1), 84.96(1) | 84.16(1) | 83.04, 83.04 | 83.04 |
| Zn1–$O_{bridging}$–Zn2 | 102.06(1), 101.44(1) | 101.75(1) | 103.11, 103.11 | 103.11 |
| $\|\alpha\|$[a] | 38.38(1), 37.17(8), 34.12(1), 36.95(0) | 36.66 | 32.50, 32.50, 34.16, 34.17 | 34.33 |

[a]Torsion angle between imidazo[1,5-a]pyridine and phenolate rings in the $IPP^-$ moiety.

For **1**, the experimental UV–vis band at 328 nm corresponds to a mixed absorption at 325 and 313 nm, starting from H-2 and H-1, arriving at L and L+1. The involved occupied orbitals are predominately composed of Cl lone pair and imidazo[1,5-a]pyridine $\pi$ contributions, while the unoccupied orbitals possess largely $\pi^*$ character of imidazo[1,5-a]pyridine or whole HIPP ligand. Therefore, these transitions can be assigned as a combination of

Table 5. Main calculated optical transitions for **1** and **2**.

| Orbital excitation | Composition | Main character | λ (nm) (Calcd) | $f$[a] | λ (nm) (exptl.) |
|---|---|---|---|---|---|
| Complex **1** | | | | | |
| 132–135 | 0.48846 | $\pi \rightarrow \pi^*$ and $n \rightarrow \pi^*$ | 325 | 0.0535 | 328 |
| 132–134 | 0.41155 | $\pi \rightarrow \pi^*$ | 313 | 0.0507 | |
| 131–135 | −0.37783 | $\pi \rightarrow \pi^*$ and $n \rightarrow \pi^*$ | | | |
| 130–134 | −0.48575 | $n \rightarrow \pi^*$ | 306 | 0.0300 | 299 (sh) |
| 133–136 | 0.49563 | $\pi \rightarrow \pi^*$ and IL | | | |
| 131–136 | 0.47770 | $\pi \rightarrow \pi^*$ | 304 | 0.0873 | |
| 132–137 | 0.63089 | $\pi \rightarrow \pi^*$ | 294 | 0.1103 | |
| 128–134 | 0.64259 | $n \rightarrow \pi^*$ | 293 | 0.0425 | |
| 130–136 | 0.39660 | $n \rightarrow \pi^*$ | 292 | 0.0428 | |
| 131–137 | 0.47101 | $\pi \rightarrow \pi^*$ | | | |
| Complex **2** | | | | | |
| 229–233 | 0.48611 | $\pi \rightarrow \pi^*$ | 428 | 0.0206 | 423 |
| 230–234 | −0.48494 | $\pi \rightarrow \pi^*$ | | | |
| 227–232 | 0.39572 | $\pi \rightarrow \pi^*$ | 382 | 0.0361 | 338 |
| 228–231 | 0.57541 | IL | | | |
| 229–235 | 0.69927 | IL | 366 | 0.0146 | |
| 229–238 | 0.45547 | $\pi \rightarrow \pi^*$ | 348 | 0.2128 | |
| 230–237 | 048,501 | $\pi \rightarrow \pi^*$ | | | |
| 225–234 | 0.47553 | $\pi \rightarrow \pi^*$ | 331 | 0.0467 | |
| 226–233 | 0.48257 | $\pi \rightarrow \pi^*$ | | | |
| 228–235 | 0.63766 | $\pi \rightarrow \pi^*$ | 324 | 0.5106 | |
| 227–236 | 0.65726 | $\pi \rightarrow \pi^*$ | 309 | 0.1713 | 299 (sh) |

[a]Oscillator strength.

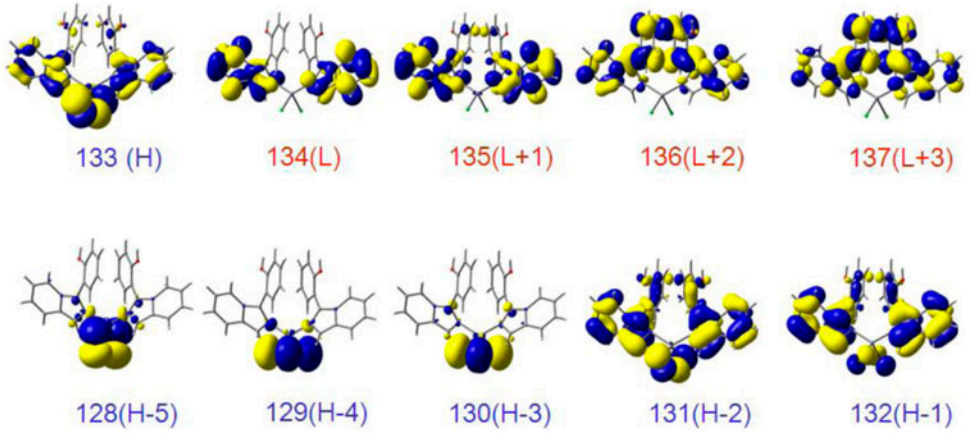


Figure 7. Relevant molecular orbitals in the absorption transitions of **1**.

$\pi \rightarrow \pi^*$ and $n \rightarrow \pi^*$. The absorption shoulder at 299 nm may come from $\pi \rightarrow \pi^*$ and $n \rightarrow \pi^*$, and intraligand (IL) transitions, relevant to the calculated bands at 292–306 nm.

Obviously, deprotonation of HIPP and coordination with metals result in the planarization and rigidification of the ligand system in dinuclear **2**. The calculated absolute value of torsional angles ($|\alpha|_{average} = 34.33°$) for **2** is also smaller than that in **1** ($|\alpha|_{average} = 50.01°$). The calculated energy gap (figure 9) between HOMO and LUMO orbitals of **2** (3.37 eV) is

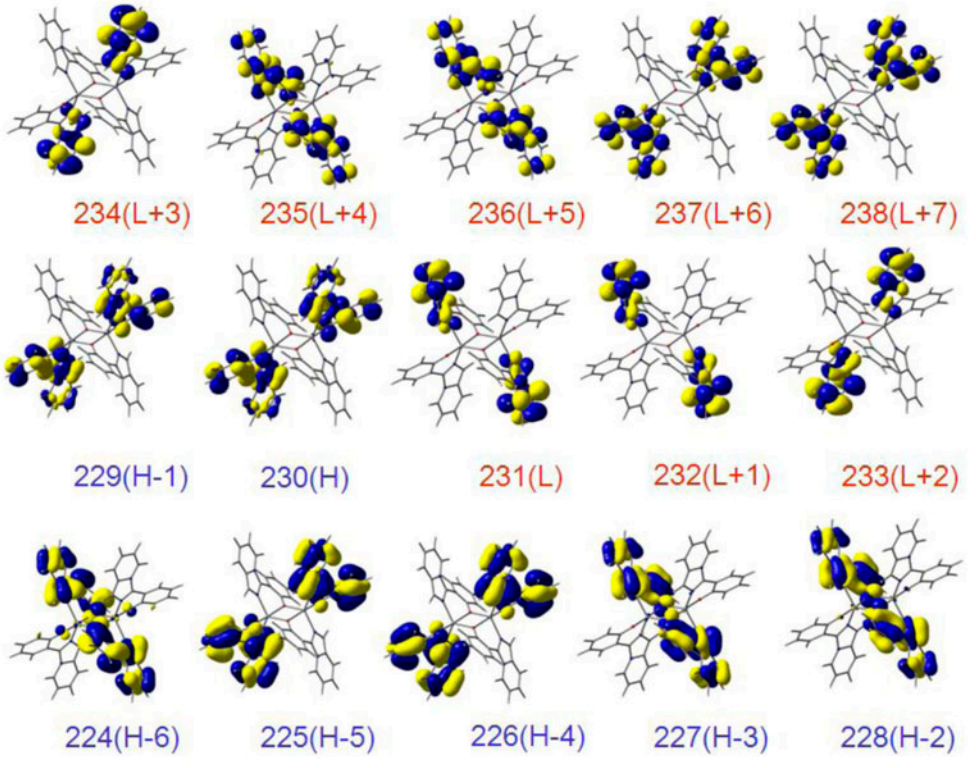


Figure 8. Relevant molecular orbitals in the absorption transitions of **2**.

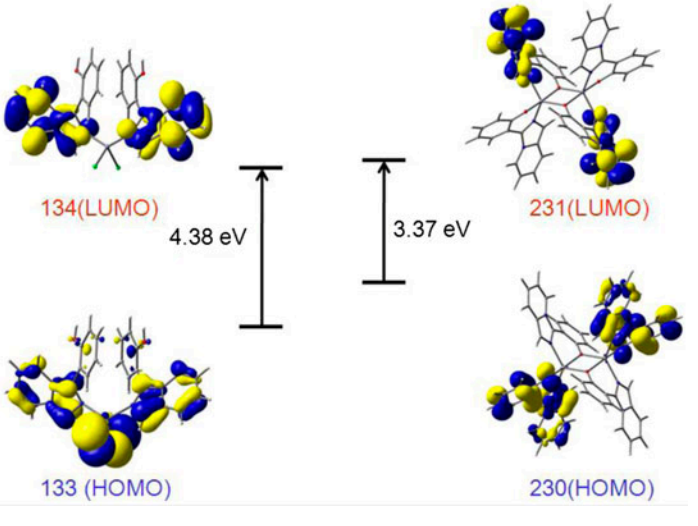


Figure 9. The energy gaps of frontier orbital for **1** and **2**.

smaller than that of **1** (4.38 eV), which may come from the dinuclear structure and the $\pi\cdots\pi$ stacking interactions.

The frontier orbitals for **2** are mainly delocalized in the whole deprotonated $IPP^-$ moiety and show essentially $\pi$ character. These orbitals appear in pairs due to the symmetrical structure. The experimental low-energy peak at 423 nm is calculated at 428 nm, attributed to $\pi\rightarrow\pi^*$, H-1→L+2, and H→L+3 transitions. The red-shifted absorption band (exptl. 338 nm) of **2** compared with **1** is well reproduced by calculations (Calcd 382, 366, 348, 331, and 324 nm, mixed). The transitions originating from H-5 to H and ending in L to L+4, L+6, and L+7 can be ascribed as $\pi\rightarrow\pi^*$ and IL transitions. The experimentally obtained absorption shoulder at 299 nm corresponds to a calculated band at 309 nm, which is attributable to H-3→L+5 transition, suggesting $\pi\rightarrow\pi^*$ character.

### 3.4. *Emission properties*

The solid-state photoluminescent spectra of HIPP and **1**–**5** have been studied at room temperature (figure 10). The free HIPP has a moderate fluorescence emission band at 421 nm upon excitation at 343 nm, attributed to ligand-centered $\pi^*\rightarrow\pi$ or $\pi^*\rightarrow n$ electronic transitions. For **1**–**3**, the emission peaks appear at 429 ($\lambda_{ex}$ = 347 nm), 476 ($\lambda_{ex}$ = 396 nm), and 417 nm ($\lambda_{ex}$ = 327 nm), respectively. The emissions of **1** and **2** are neither metal-to-ligand charge transfer nor ligand-to-metal charge transfer, since $Zn^{II}$ ions are difficult to oxidize or reduce due to their $d^{10}$ configuration [35–37]. Thus, the luminescent bands of **1** and **2** can probably be ascribed to intraligand electron transition, since very similar emissions are also observed for the free ligand [38–41]. The emission of **3** shows red-shift (55 nm) compared with the free ligand. Similar to that observed in the absorption spectra, this red-shift may be assigned to the highly resonant $\pi$-conjugated framework of the deprotonated HIPP ligand, giving a decrease in the $\pi\rightarrow\pi^*$ energy gap of the ligand molecular orbitals responsible for the transitions [42, 43]. The emission of **3** exhibits a slight blue-shift (4 nm) with respect to free HIPP ligand, which may be attributed to the coordination of HIPP [44, 45]. Unlike **3**, no obvious

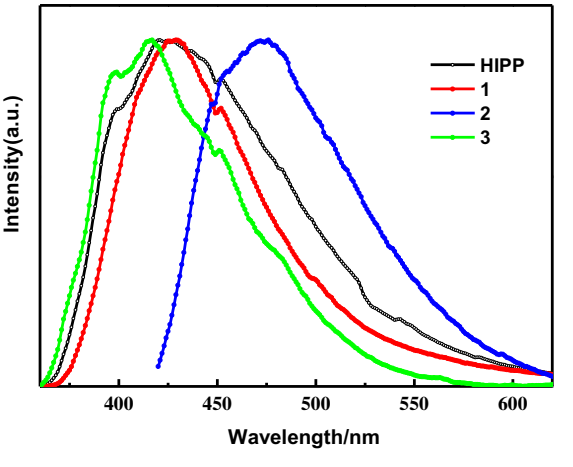


Figure 10. Emission spectra of HIPP, **1**, **2** and **3** in the solid state at room temperature.

emission for **4** and **5** was observed at room temperature. The luminescence of **4** and **5** may be quenched by the coordination of $Co^{II}$ ions with the deprotonated ligand [46–48].

### 3.5. *Magnetic properties of 3–5*

Variable-temperature dc magnetic susceptibility data were recorded for polycrystalline samples of **3**–**5** at an applied magnetic field of 1000 Oe from 2 to 300 K.

The $\chi_M T$ value of **3** at 300 K is 5.35 $cm^3$ K $M^{-1}$ (figure 11), which is larger than the spin-only value of 3.76 $cm^3$ K $M^{-1}$ expected for two $S = 3/2$ uncoupled spins, possibly due to the orbital contributions of the metal ions [49–52]. As the temperature is lowered, the $\chi_M T$ value decreases gradually to a minimum of 2.91 $cm^3$ K $M^{-1}$ at 2 K. This behavior is indicative of antiferromagnetic exchange interactions between the metal ions. The reciprocal magnetic susceptibilities from 25 to 300 K follow the Curie–Weiss Law of $1/\chi_M = (T-\theta)/C$ with a Curie constant $C$ of 5.93 $cm^3$ K $M^{-1}$ and a Weiss constant $\theta$ of −34.03 K, which confirm the existence of weak antiferromagnetic interactions between the metal centers.

The value of $\chi_M T$ for **4** is 8.57 $cm^3$ K $M^{-1}$ at 300 K (figure 12), which is larger than the sum of the expected value (5.62 $cm^3$ K $M^{-1}$, $g = 2.0$, $S = 3/2$) for three uncoupled high-spin $Co^{II}$ ions [53–55]. As the temperature lowered, the $\chi_M T$ value first increases smoothly and then rises abruptly to a maximum value of 12.38 $cm^3$ K $M^{-1}$ at 5.4 K, and sharply decreases to a minimum value of 11.1 $cm^3$ K $M^{-1}$ at 2 K. Fitting the data at 25–300 K with the Curie–Weiss law gives a $C$ of 8.48 $cm^3$ K $M^{-1}$ and a $\theta$ of 3.79 K. The $C$ value is consistent with the value of 8.57 $cm^3$ K $M^{-1}$ at 300 K. The positive value of $\theta$ indicates very weak ferromagnetic couplings between $Co^{II}$ ions.

For **5**, the $\chi_M T$ value of 4.93 $cm^3$ K $M^{-1}$ per Co2 unit at 300 K is much larger than expected for two magnetically isolated high-spin $Co^{II}$ ions (3.76 $cm^3$ K $M^{-1}$) with $S = 3/2$, revealing a significant orbital contribution. Upon lowering the temperature, the $\chi_M T$ value first slowly decreases to 3.22 $cm^3$ K $M^{-1}$ at 28 K and then rapidly decreases to a value of 0.28 $cm^3$ K $M^{-1}$ at 2 K (figure 13). The magnetic susceptibility from 15 to 300 K obeys the Curie–Weiss law with a Weiss constant $\theta$ of −18.33 K and a Curie constant $C$ of 5.20 $cm^3$

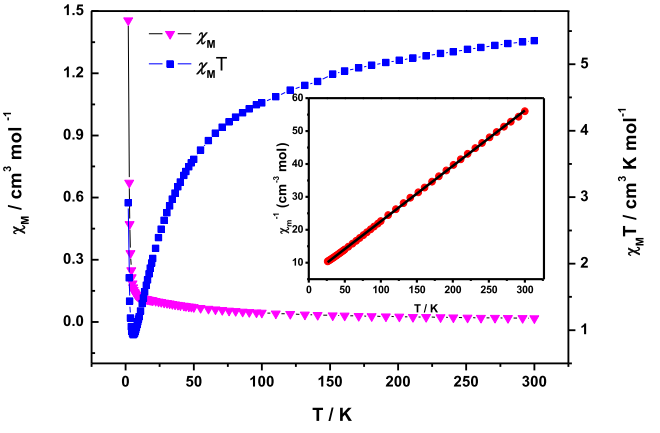


Figure 11. Temperature dependence of magnetic susceptibilities in the form of $\chi_M T$ *vs.* $T$ and $\chi_M$ *vs.* $T$ for **3** at 1 kOe. Inset: temperature dependence of magnetic susceptibilities in the form of $\chi_M^{-1}$ *vs.* $T$ for **3** at 1 kOe. The solid line in the graph of the inset corresponds to the best fit from 300 to 25 K.

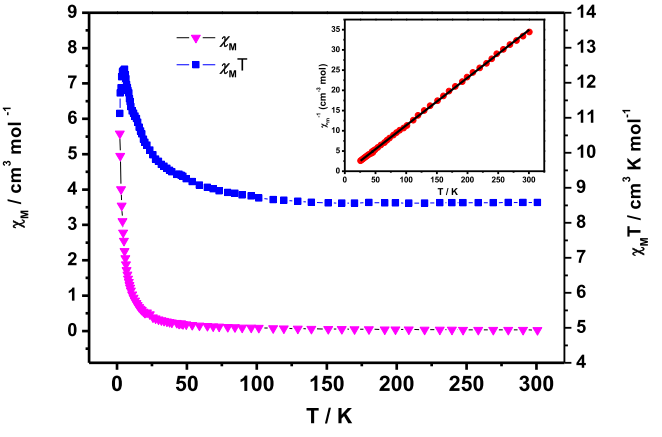


Figure 12. Temperature dependence of magnetic susceptibilities in the form of $\chi_M T$ *vs.* $T$ and $\chi_M$ *vs.* $T$ for **4** at 1 kOe. Inset: temperature dependence of magnetic susceptibilities in the form of $\chi_M^{-1}$ *vs.* $T$ for **4** at 1 kOe. The solid line in the graph of the inset corresponds to the best fit from 300 to 25 K.

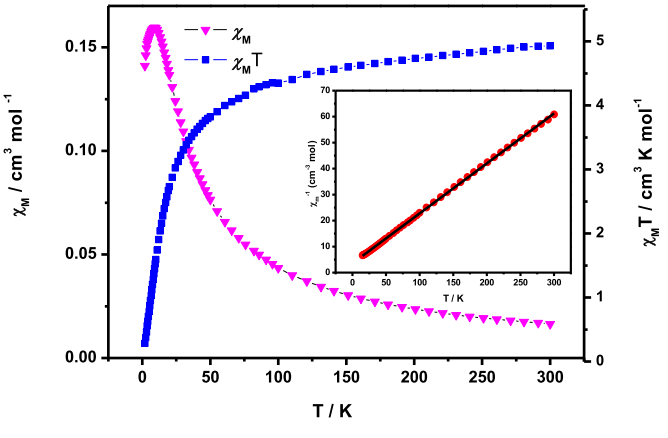


Figure 13. Temperature dependence of magnetic susceptibilities in the form of $\chi_M T$ *vs.* $T$ and $\chi_M$ *vs.* $T$ for **5** at 1 kOe. Inset: temperature dependence of magnetic susceptibilities in the form of $\chi_M^{-1}$ *vs.* $T$ for **5** at 1 kOe. The solid line in the graph of the inset corresponds to the best fit from 300 to 15 K.

K $M^{-1}$. The decrease of the $\chi_M T$ value or the negative $\theta$ value can be induced by antiferromagnetic coupling interactions within the chain.

### 3.6. *Powder X-ray diffraction*

PXRD for **1**–**5** was used to confirm the phase purity of the bulk sample. As shown in figure S2, all the peaks presented in the measured patterns closely match the simulated patterns generated from single diffraction data, indicating the phase purity of the complexes.

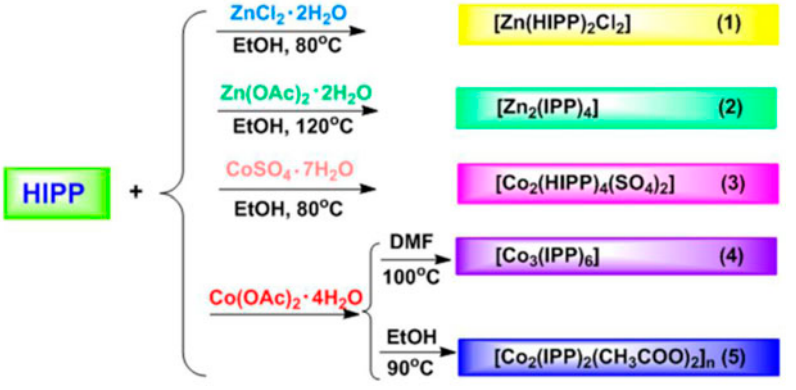


Scheme 1. Syntheses of **1**–**5**.

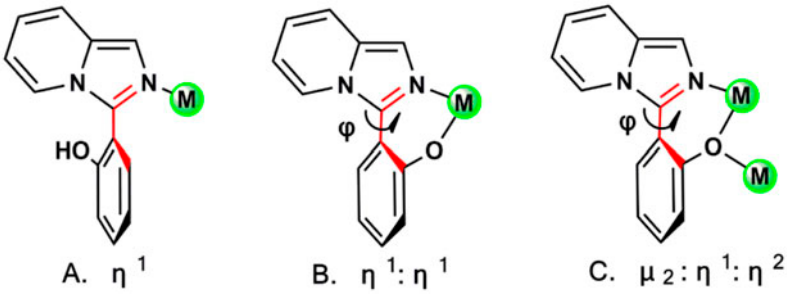


Scheme 2. Coordination modes of the HIPP and $IPP^{-}$ in **1**–**5**.

## 4. Conclusion

We have synthesized five complexes supported by HIPP, a derivative of imidazo[1,5-a]pyridine, under hydrothermal conditions. This is the first report of coordination complexes based on HIPP. The diverse coordination modes indicate that the HIPP can offer powerful chelating abilities. Moreover, these results illustrate that appropriate metal salts and solvents play important roles in assembling various coordination structures. The UV–vis and luminescent properties for **1**–**5** and magnetic properties for **3**–**5** are studied. DFT and TDDFT calculations have been used to interpret their electronic properties. The studies for employing HIPP and its analogs to produce novel polynuclear clusters with esthetically pleasing topologies by adding other auxiliary ligands are currently underway in our laboratory.

## Supplementary material

Tables S1–S5 give bond lengths and angles for **1**–**5**. Figure S1 gives the calculated absorption spectra for **1** and **2**. Figure S2 gives the XRD spectra for **1**–**5**. Figures S3–S8 give the IR spectra for HIPP and **1**–**5**. Tables S6 and S7 give the optimized Cartesian coordinated

for **1** and **2**. CCDC reference numbers 951367, 951368, 951364, 951365, and 951366 for **1**–**5**, respectively. These data can be obtained free of charge from The Cambridge Crystallographic Data Center via http://www.ccdc.cam.ac.uk/data_request/cif, by e-mailing data_request@ccdc.cam.ac.uk or by contacting the Cambridge Crystallographic Data Center, 12 Union Road, Cambridge CB2 IEZ, UK; Fax:+44(0)1223 336033.

## Funding

The authors appreciate the financial support from the Natural Science Foundation of China [grant number 21272167] and [grant number 21201127], a project funded by the Priority Academic Program Development of Jiangsu Higher Education Institution, and the Graduate Education Innovation Project in Jiangsu Province [grant number CXZZ12_0808] and [grant number CXLX12_0784].

## References

[1] C. Garino, T. Ruiu, L. Salassa, A. Albertino, G. Volpi, C. Nervi, R. Gobetto, K.I. Hardcastle. *Eur. J. Inorg. Chem.*, **2008**, 3587 (2008).
[2] L. Salassa, C. Garino, A. Albertino, G. Volpi, C. Nervi, R. Gobetto, K.I. Hardcastle. *Organometallics*, **27**, 1427 (2008).
[3] H. Nakamura, H. Yamamoto. *Chem. Abstr.*, **142**, 440277 (2005).
[4] H. Matsumoto, K. Ikeda, N. Nagata, H. Takayanagi, Y. Mizuno, M. Tanaka, T. Sasaki. *J. Med. Chem.*, **42**, 1661 (1999).
[5] A. Kamal, G. Ramakrishna, P. Raju, A.V.S. Rao, A. Viswanath, V.L. Nayak, S. Ramakrishna. *Eur. J. Med. Chem.*, **46**, 2427 (2011).
[6] D. Kim, L. Wang, J.J. Hale, C.L. Lynch, R.J. Budhu, M. MacCoss, S.G. Mills, L. Malkowitz, S.L. Gould, J.A. DeMartino, M.S. Springer, D. Hazuda, M. Miller, J. Kessler, R.C. Hrin, G. Carver, A. Carlla, K. Henry, J. Lineberger, W.A. Schleif, E.A. Emini. *Bioorg. Med. Chem. Lett.*, **15**, 2129 (2005).
[7] M.L. Bode, D. Gravestock, S.S. Moleele, C.W. van der Westhuyzen, S.C. Pelly, P.A. Steenkamp, H.C. Hoppe, T. Khan, L.A. Nkabinde. *Bioorg. Med. Chem.*, **19**, 4227 (2011).
[8] M. Alcarazo, S.J. Roseblade, A.R. Cowley, R. Fernández, J.M. Brown, J.M. Lassaletta. *J. Am. Chem. Soc.*, **127**, 3290 (2005).
[9] S.J. Roseblade, A. Ros, D. Monge, M. Alcarazo, E. Álvarez, J.M. Lassaletta, R. Fernández. *Organometallics*, **26**, 2570 (2007).
[10] F.E. Hahn. *Angew. Chem. Int. Ed.*, **45**, 1348 (2006).
[11] N. Kundu, M. Maity, P.B. Chatterjee, S.J. Teat, A. Endo, M. Chaudhury. *J. Am. Chem. Soc.*, **133**, 20104 (2011).
[12] Y.M. Chen, L. Li, Y.Y. Cao, J. Wu, Q. Gao, Y.H. Li, H.L. Hu, W. Liu, Y.L. Liu, Z.K. Kang, J.P. Li. *CrystEngComm*, **15**, 2675 (2013).
[13] Y.M. Chen, L. Li, Z. Chen, Y.L. Liu, H.L. Hu, W.Q. Chen, W. Liu, Y.H. Li, T. Lei, Y.Y. Cao, Z.H. Kang, M.S. Lin, W. Li. *Inorg. Chem.*, **51**, 9705 (2012).
[14] J.J. Wu, M.L. Cao, B.H. Ye. *Chem. Commun.*, **46**, 3687 (2010).
[15] A.G.J. Ligtenbarg, A.L. Spek, R. Hage, B.L. Feringa. *J. Chem. Soc., Dalton Trans.*, 659 (1999).
[16] C.M. Álvarez, L. Álvarez-Miguel, R. García-Rodríguez, D. Miguel. *Dalton Trans.*, 7041 (2012).
[17] A. Douhal, F. Amat-Guerri, A.U. Acuña. *J. Phys. Chem.*, **99**, 76 (1995).
[18] G.M. Sheldrick. *SHELXS-97, Program for Crystal Structure Solution*, University of Göttingen, Germany (1997).
[19] G.M. Sheldrick. *SHELXL-97, Program for the Refinement of Crystal Structures from Diffraction Data*, University of Göttingen, Germany (1997).
[20] M.J. Frisch, G.W. Trucks, H.B. Schlegel. *Gaussian 03 (Revision B.04)*, Gaussian, Inc., Wallingford, CT (2004). The full citation is given in the Supplementary Material.
[21] C. Lee, W.T. Yang, R.G. Parr. *Phys. Rev. B*, **37**, 785 (1988).
[22] B. Miehlich, A. Savin, H. Stoll, H. Preuss. *Chem. Phys. Lett.*, **157**, 200 (1989).
[23] A.D. Becke. *J. Chem. Phys.*, **98**, 5648 (1993).
[24] G.E. Zervaki, M.S. Roy, M.K. Panda, P.A. Angaridis, E. Chrissos, G.D. Sharma, A.G. Coutsolelos. *Inorg. Chem.*, **52**, 9813 (2013).
[25] C. Öztürk, K. Topal, V. Aviyente. *J. Org. Chem.*, **70**, 7080 (2005).

[26] X.G. Bao, D.A. Hrovat, W.T. Borden. *J. Org. Chem.*, **77**, 956 (2012).
[27] W.J. Hehre, L. Radom, P.V.R. Schleyer, J.A. Pople. *Ab Initio Molecular Orbital Theory*, Wiley-Interscience, New York (1986).
[28] T. Clark. *A Handbook of Computational Chemistry*, Wiley-Interscience, New York (1985).
[29] T.H. Dunning, P.J. Hay. In *Modern Theoretical Chemistry*, H.F. Schaefer III (Ed.), Vol. 3, p. 1, Plenum Press, New York (1976).
[30] P.J. Hay, W.R. Wadt. *J. Chem. Phys.*, **82**, 270, 284, 299 (1985).
[31] J.M. Crawforth, M. Paoletti. *Tetrahedron Lett.*, **50**, 4916 (2009).
[32] A.G. Orpen, L. Brammer, F.H. Allen, O. Kennard, D.G. Watson, R. Taylor. *J. Chem. Soc., Dalton Trans.*, S1 (1989).
[33] W. Addison, T.N. Rao, J. Reedijk, J. van Rijn, G.C. Verschoor. *J. Chem. Soc., Dalton Trans.*, 1349 (1984).
[34] N. Kundu, S.M.T. Abtab, S. Kundu, A. Endo, S.J. Teat, M. Chaudury. *Inorg. Chem.*, **51**, 2652 (2012).
[35] D. Dey, S. Roy, R.N.D. Purkayastha. *J. Coord. Chem.*, **64**, 1165 (2011).
[36] Z.F. Chen, R.G. Xiong, J. Zhang, X.T. Chen, Z.L. Xue, X.Z. You. *Inorg. Chem.*, **40**, 4075 (2001).
[37] B. Liu, G.P. Yang, Y.Y. Wang, R.T. Liu, L. Hou, Q.Z. Shi. *Inorg. Chim. Acta*, **367**, 127 (2011).
[38] H.F. Zhu, J. Fan, T.A. Okamura, W.Y. Sun, N. Ueyama. *Cryst. Growth Des.*, **5**, 289 (2005).
[39] J.K. Xu, X.C. Sun, C.X. Ju, L.R. Yang, C.F. Bi, M. Sun. *J. Coord. Chem.*, **66**, 2693 (2013).
[40] Y.Y. Liu, Y.Q. Huang, W. Shi, P. Cheng, D.Z. Liao, S.P. Yan. *Cryst. Growth Des.*, **7**, 1483 (2007).
[41] J.K. Xu, X.C. Sun, C.X. Ju, J. Sheng, F. Wang, M. Sun. *J. Coord. Chem.*, **66**, 2541 (2013).
[42] Q. Su, W. Gao, Q.L. Wu, L. Ye, G.H. Li, Y. Mu. *Eur. J. Inorg. Chem.*, **2007**, 4168 (2007).
[43] C.S.B. Gomes, P.T. Gomes, M.T. Duarte, R.E.D. Paolo, A.L. Macantita, M.J. Calhorda. *Inorg. Chem.*, **48**, 11176 (2009).
[44] M. Shu, C. Tu, W.D. Xu, H.B. Jin, J. Sun. *Cryst. Growth Des.*, **6**, 1890 (2006).
[45] H.Y. Bai, J.F. Ma, J. Yang, Y.Y. Liu, H. Wu, J.C. Ma. *Cryst. Growth Des.*, **10**, 995 (2010).
[46] L. Zhang, W.W. Chen, Y.Y. Ge, Y. Ling, X.P. Ouyang, J. Li, M. Du. *Inorg. Chim. Acta*, **363**, 866 (2010).
[47] X.L. Wang, Y.Q. Chen, G.C. Liu, H.Y. Lin, W.Y. Zheng, J.X. Zhang. *J. Organomet. Chem.*, **694**, 2263 (2009).
[48] Z.D. Lu, L.L. Wen, Z.P. Ni, Y.Z. Li, H.Z. Zhu, Q.J. Meng. *Cryst. Growth Des.*, **7**, 268 (2007).
[49] A.K. Boudalis, C.P. Raptopoulou, B. Abarca, R. Ballesteros, M. Chadlaoui, J.P. Tuchagues, A. Terzis. *Angew. Chem. Int. Ed.*, **45**, 432 (2006).
[50] X.N. Cheng, W.X. Zhang, Y.Z. Zheng, X.M. Chen. *Chem. Commun.*, **34**, 3603 (2006).
[51] M.L. Han, N. Ma, S.H. Li. *J. Coord. Chem.*, **42**, 976 (2012).
[52] T. Yi, C. Ho-Chol, S. Gao, S. Kitagawa. *Eur. J. Inorg. Chem.*, **2006**, 1381 (2006).
[53] L. Zhang, W. Gao, Q.L. Wu, Q. Su, J.S. Zhang, Y. Mu. *J. Coord. Chem.*, **66**, 3182 (2013).
[54] X.Y. Zhang, Z.Y. Liu, Y.F. Xia, Y.Y. Zhang, E.C. Yang, X.J. Zhao. *J. Coord. Chem.*, **66**, 4399 (2013).
[55] X.M. Qiu, S.N. Wang, J. Lu, L.Q. Kong, D.C. Li, J.M. Dou. *J. Coord. Chem.*, **65**, 3308 (2012).